
Contents

1	Simulating Cosmological Evolution with Enzo	3
	<i>Michael L. Norman, James Bordner, Daniel Reynolds and Rick Wagner, Greg L. Bryan, Robert Harkness, and Brian O'Shea</i>	
1.1	Cosmological structure formation	3
1.2	The Enzo code	6
1.2.1	Physical model and numerical algorithms	6
1.2.2	Adaptive mesh refinement	7
1.2.3	Implementation	8
1.2.4	Parallelization	9
1.2.5	Fast sibling grid search	10
1.2.6	Enzo I/O	11
1.3	Performance and scaling on terascale platforms	12
1.3.1	Unigrid application	12
1.3.2	AMR application	13
1.3.3	Parallel scaling	16
1.4	Toward petascale Enzo	16
1.4.1	New AMR data structures	16
1.4.2	Hybrid parallelism	18
1.4.3	Implicitly-coupled radiation hydrodynamics	19
1.4.4	Inline analysis tools	19
1.5	Acknowledgements	21
	References	23



Chapter 1

Simulating Cosmological Evolution with Enzo

Michael L. Norman, James Bordner, Daniel Reynolds and Rick Wagner

Laboratory for Computational Astrophysics, Center for Astrophysics and Space Sciences, University of California San Diego, 9500 Gilman Dr., La Jolla CA 92093, (mlnorman, jobordner, drreynolds, rpwagner)@ucsd.edu

Greg L. Bryan

Astronomy Department, Columbia University, 550 West 120th St., New York NY 10027, gbryan@astro.columbia.edu

Robert Harkness

San Diego Supercomputer Center, 9500 Gilman Dr., La Jolla CA 92093, harkness@sdsc.edu

Brian O'Shea

Theoretical Astrophysics (T-6), Los Alamos National Laboratory, P.O. Box 1663, Los Alamos, NM 87545, bwoshea@lanl.gov

1.1	Cosmological structure formation	3
1.2	The Enzo code	4
1.3	Performance and scaling on terascale platforms	12
1.4	Toward petascale Enzo	16
1.5	Acknowledgements	20

1.1 Cosmological structure formation

The universe is homogeneous and isotropic on scales exceeding half a billion light years, but on smaller scales it is clumpy, exhibiting a hierarchy of structures ranging from individual galaxies up to groups and clusters of galaxies, and on the largest scales, the galaxies are aligned in a cosmic web of filaments and voids. In between the galaxies is a diffuse plasma which is the reservoir of matter out of which galaxies form. Understanding the origin and evolution of these structures is the goal of *cosmological structure formation* (CSF).

It is now understood that CSF is driven by the gravitational clustering of dark matter, the dominant mass constituent of the universe. Slight inhom-

geneities in the dark matter distribution laid down in the early universe seed CSF. The rate at which structure develops in the universe depends upon the power spectrum of these perturbations, now well measured on scales greater than one million light years [1]. It also depends on the cosmic expansion rate, which in turn is influenced by dark energy, a form of energy which exhibits negative pressure and whose existence was revealed only in 1998 by the discovery that the expansion rate is accelerating. The quantitative study of CSF is thus a direct route to studying two of the most mysterious substances in modern physics: dark matter and dark energy.

The part of the universe that astronomers can see directly is made up of ordinary “baryonic” matter. Thus, in order to make contact with observations, we must simulate the detailed dynamics and thermodynamics of the cosmic plasma—mostly hydrogen and helium—under the influence of dark matter and dark energy, as well as ionizing radiation backgrounds. Such simulations are called hydrodynamic cosmological simulations, and are what we consider in this chapter. CSF is inherently nonlinear, multidimensional, and involves a variety of physical processes operating on a range of length- and time-scales. Large scale numerical simulation is the primary means we have of studying it in detail.

To give a feeling for the range of scales involved, the large scale distribution of galaxies in the present universe traces out a web-like pattern on typical scales of 100 million light years. Individual galaxies are 10^{3-4} times smaller in linear scale. Resolving the smallest galaxies with ten resolution elements per radius yields a range of scales of 2×10^5 throughout the large scale volume. A uniform grid of this size in 3D is out of the question, now and in the near future. However, such a high dynamic range is not needed everywhere, but only where the galaxies are located. Using adaptive mesh refinement (AMR) techniques we are close to achieving this dynamic range running on today’s terascale computers including a simple description of the baryonic fluid (Fig. 1.1). With petascale platforms, even higher dynamic ranges will be achievable including the complex baryonic physics that governs the formation and evolution of galaxies.

In this paper we describe **Enzo**[2] a multiphysics, parallel, AMR application for simulating CSF developed at UCSD and Columbia. We describe its physics, numerical algorithms, implementation, and performance on current terascale platforms. We also discuss our future plans and some of the challenges we face as we move to the petascale.

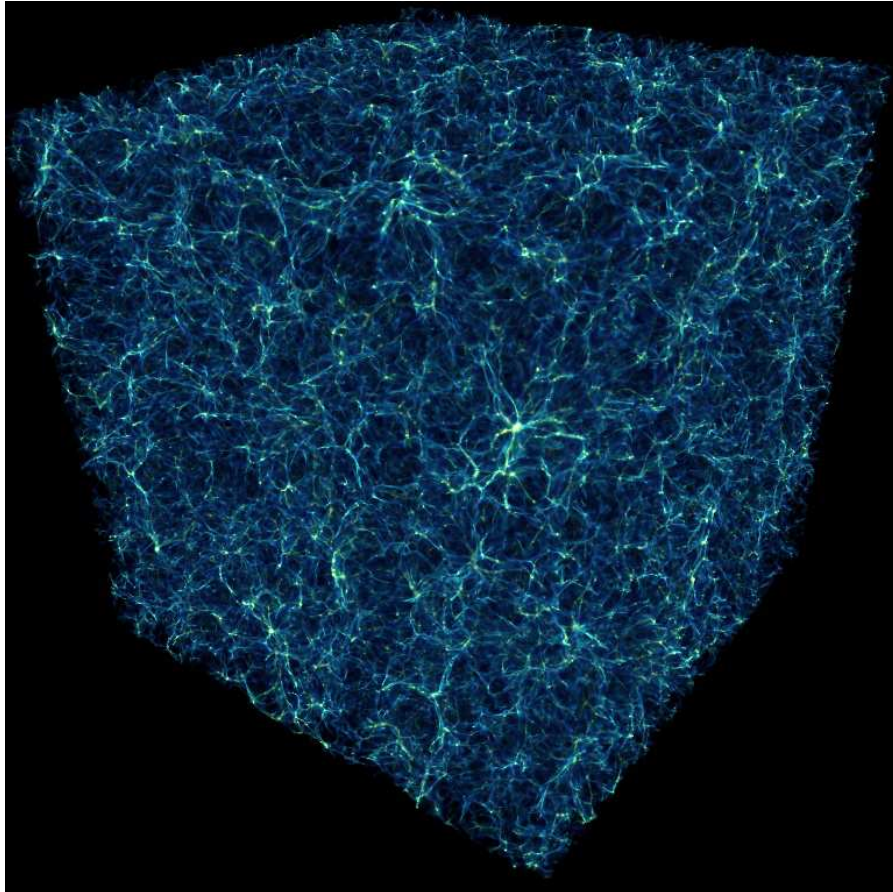


FIGURE 1.1: Enzo hydrodynamic simulation of cosmic structure in a 700 Mpc volume of the universe. Up to seven levels of adaptive mesh refinement resolve the distribution of baryons within and between galaxy clusters, for an effective resolution of $65,536^3$. Volume rendering of baryon density. Image credit: M. Hall, NCSA

1.2 The Enzo code

1.2.1 Physical model and numerical algorithms

Matter in the universe is of two basic types: baryonic matter composed of atoms and molecules out of which stars and galaxies are made, and non-baryonic “dark” matter of unknown composition, which is nevertheless known to be the dominant mass constituent in the universe on galaxy scales and larger. **Enzo** self-consistently simulates both components, which evolve according to different physical laws and therefore require different numerical algorithms.

Baryonic matter is evolved using a finite volume discretization of the Euler equations of gas dynamics cast in a frame which expands with the universe. Energy source and sink terms due to radiative heating and cooling processes are included, as well as changes in ionization state of the gas [3]. We use the Piecewise Parabolic Method (PPM), which is a higher-order Godunov scheme developed by Colella and Woodward for ideal gas dynamics calculations [4]. The species abundances for H, H⁺, He, He⁺, He⁺⁺, and e⁻ (and optionally H₂, HD and related species) are solved out of equilibrium by integrating the rate equations including radiative and collisional processes [3]. Radiation fields are modeled as evolving but spatially homogeneous backgrounds using published prescriptions.

Dark matter is assumed to behave as a collisionless phase fluid, obeying the Vlasov-Poisson equation. Its evolution is solved using particle-mesh algorithms for collisionless N-body dynamics [5]. In particular, we use the spatially second order-accurate Cloud-in-Cell (CIC) formulation, together with leapfrog time integration, which is formally second order-accurate in time. Dark matter and baryonic matter interact only through their self-consistent gravitational field. The gravitational potential is computed by solving the Poisson equation on the uniform or adaptive grid hierarchy using Fast Fourier Transform and multigrid techniques. In generic terms, **Enzo** is a 3D hybrid code consisting of a multi-species hydrodynamic solver for the baryons coupled to a particle-mesh solver for the dark matter via a Poisson solver.

Matter evolution is computed in a cubic domain of length $L = a(t)X$, where X is the domain size in comoving coordinates, and $a(t)$ is the homogenous and isotropic scale factor of the universe which is an analytic or numerical solution of the Friedmann equation, a first order ODE. For sufficiently large X compared to the structures of interest, any chunk of the universe is statistically equivalent to any other, justifying the use of periodic boundary conditions. The speed of FFT algorithms and the fact that they are ideally suited to periodic problems make them the Poisson solver of choice given the large grids employed— 1024^3 or larger.

CSF simulations require very large grids and particle numbers due to two

competing demands: large boxes are needed for a fair statistical sample of the universe; and high mass and spatial resolutions are needed to adequately resolve the scale lengths of the structures which form. For example, in order to simultaneously describe galaxies' large scale distribution in space (large scale structure) and adequately resolve their internal structure, a dynamic range of 10^5 per spatial dimension and 10^9 in mass is needed *at a minimum*, as discussed above.

1.2.2 Adaptive mesh refinement

The need for higher resolution than afforded by uniform grids motivated the development of **Enzo**. **Enzo** uses structured adaptive mesh refinement (SAMR, [6, 7]) to achieve high resolution in gravitational condensations. The central idea behind SAMR is simple to describe but challenging to implement efficiently on parallel computers. The idea is this: while solving the desired set of equations on a coarse uniform grid, monitor the quality of the solution and when necessary, add an additional, finer mesh over the region that requires enhanced resolution. This finer (child) mesh obtains its boundary conditions from the coarser (parent) grid or from other neighboring (sibling) grids with the same mesh spacing. The finer grid is also used to improve the solution on its parent. In order to simplify the bookkeeping, refined patches are required to have a cell spacing which is an integer number divided by the parent's spacing. In addition, refined patches must begin and end on a parent cell boundary. As the evolution continues, it may be necessary to move, resize or even remove the finer mesh. Refined patches themselves may require further refinement, producing a tree structure that can continue to any depth. We denote the level of a patch by the number of times it has been refined compared to the root grid. If the cell spacing of the root grid (level 0) is Δx , then the cell spacing of a mesh at level l is $\Delta x/r^l$ where r is the integer refinement factor (typically 2).

To advance our system of coupled equations in time on this grid hierarchy, we use a recursive algorithm. The `EvolveLevel` routine is passed the level of the hierarchy it is to work on and the new time. Its job is to march the grids on that level from the old time to the new time:

Inside the loop which advances the grids on this level, there is a recursive call so that all the levels with finer subgrids are advanced as well. The resulting order of timesteps is like the multigrid W-cycle.

Before we update the hyperbolic gas dynamics equations and solve the elliptic Poisson equation, we must set the boundary conditions on the grids. This is done by first interpolating from a grid's parent and then copying from sibling grids, where available. Once the boundary values have been set, we solve the Poisson equation using the procedure `PrepareDensityField` and evolve the hydrodynamic field equations using procedure `SolveHydroEquations`. The multispecies kinetic equations are integrated by procedure `SolveRateEquations`, followed by an update to the gas energy equation due to radiative cooling by

```

EvolveLevel(level, ParentTime)
begin
  SetBoundaryValues(all grids)
  while (Time < ParentTime)
  begin
    dt = ComputeTimeStep(all grids)
    PrepareDensityField(all grids, dt)
    SolveHydroEquations(all grids, dt)
    SolveRateEquations(all grids, dt)
    SolveRadiativeCooling(all grids, dt)
    Time += dt
    SetBoundaryValues(all grids)
    EvolveLevel(level+1, Time)
    RebuildHierarchy(level+1)
  end
end

```

FIGURE 1.2: Enzo AMR algorithm.

procedure `SolveRadiativeCooling`. The final task of the `EvolveLevel` routine is to modify the grid hierarchy to reflect the changing solution. This is accomplished via the `RebuildHierarchy` procedure, which takes a level as an argument and modifies the grids on that level and all finer levels. This involves three steps: First, a refinement test is applied to all the grids on that level to determine which cells need to be refined. Second, rectangular regions are chosen which cover all of the refined regions, while attempting to minimize the number of unnecessarily refined points. Third, the new grids are created and their values are copied from the old grids (which are deleted) or interpolated from parent grids. This process is repeated on the next refined level until the grid hierarchy has been entirely rebuilt.

1.2.3 Implementation

`Enzo` is written in a mixture of C++ and Fortran. High-level functions and data structures are implemented in C++ and computationally intensive lower-level functions are implemented in Fortran. As described in more detail below, `Enzo` is parallelized using the MPI message-passing library [8] and uses the HDF5 data format [9] to write out data and restart files in a platform-independent format. The code is quite portable and has been run on numerous parallel shared and distributed memory systems, including the IBM Power N systems, SGI Altix, Cray XT3, IBM BG/L, and numerous Beowulf-style linux clusters.

The AMR grid patches are the primary data structure in `Enzo`. Each individual patch is treated as a separate object, and can contain both field

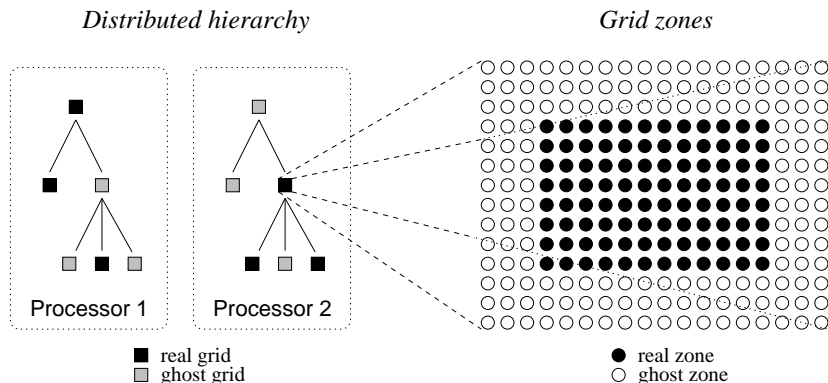


FIGURE 1.3: Real and ghost grids in a hierarchy; real and ghost zones in a grid.

variables and particle data. Individual patches are organized into a dynamic distributed AMR mesh hierarchy using two different methods: the first is a hierarchical tree and the second is a level-based array of linked lists. This allows grids to be quickly accessed either by level or depth in the hierarchy. The tree structure of a small illustrative 2D AMR hierarchy – six total grids in a three level hierarchy distributed across two processors – is shown on the left in Figure 1.3.

Each data field within a grid is an array of zones of 1,2 or 3 dimensions (typically 3D in cosmological structure formation). Zones are partitioned into a core block of *real zones* and a surrounding layer of *ghost zones*. Real zones are used to store the data field values, and ghost zones are used to temporarily store neighboring grid values when required for updating real zones. The ghost zone layer is three zones deep in order to accommodate the computational stencil of the hydrodynamics solver, as indicated in the right panel in Figure 1.3. These ghost zones can lead to significant computational and storage overhead, especially for the smaller grid patches that are typically found in the deeper levels of an AMR grid hierarchy.

1.2.4 Parallelization

Parallelization is achieved by distributing the patches, with each grid object locally resident in memory. Communication between grids on different processors is carried out using message-passing. The structure of the hierarchy, in the form of the set of linked lists described earlier, is stored redundantly on every processor to facilitate communication. However, if we kept all the grid data on all processors that would obviously consume too much memory, so instead we have developed the concept of a *ghost grid*, which is a nearly empty grid structure used to represent those grids that reside on other processors. For every *real grid*, which contains all grid data and resides on a given proces-

sor, there are $p - 1$ *ghost grids* which represent that grid on other processors (assuming p processors). This is feasible because *ghost grids* consume orders of magnitude less memory than *real grids* (but see below for a discussion of how this must change for very large numbers of processors). This structure is shown graphically in Figure 1.3.

Since child grids depend on parent grids, parallelization can only proceed over the grids on a given level (different levels must be computed in a serial fashion). Therefore, all grids on a given level are distributed over processors separately, starting with the root grid. The root grid is simply tiled and split into a number of patches which is at least as large as the number of processors. Then, as grids are added, each grid is placed by default on the same processor as its parent, minimizing communication. Once the rebuild of the hierarchy has completed on a given level, the load balancing ratio between processors is computed and grids are transferred between processors in an attempt to even the load. Because grids are discrete objects, this cannot in general be done in an optimal fashion (although we have experimented with grid splitting, see [10]). For the large problems typical of CSF, there are many grids per processor so this is not typically a problem.

Communication is overlapped with computation by pre-computing communication pathways and starting non-blocking MPI calls. Care is taken to generate these as soon as possible so that the data will be ready when required by another processor. This is one of the reasons why it is important to have the entire hierarchy in memory on each processor, so that all grid overlaps can be found and data transfer initiated early in the compute cycle.

1.2.5 Fast sibling grid search

As the code has been expanded and run on more and more processors with more and more grids, a number of performance bottlenecks have been identified and eliminated. We describe one such example here. Many binary operations between grids, such as copying boundary values, require first identifying which grids overlap. In early versions of the code, this was done using a simple double-loop to perform a comparison between each grid and all other grids. This is an $O(N_{\text{grid}}^2)$ operation but because the number of operations per grid comparison is very small, this bottleneck did not appear until we ran simulations with 100's of processors, generating more than 10,000 grids.

The problem was solved by carrying out a chaining-mesh search to identify neighboring grids. First, a coarse mesh is constructed over the entire domain (with 4^3 times fewer cells than the root grid), and a linked list is begun for each chaining-mesh cell. Then we loop over all the grids and find which chaining-mesh cell(s) that grid belongs to, adding that grid to the appropriate linked list(s). In this way we generate a coarse localization of the grids, so that when we need to find the list of neighbors for a given grid, we simply need to check the grids in the same chaining-mesh (or multiple chaining-meshes if the grid covers more than one) This reduces the number of comparisons by a factor of

about N_{chain}^{-3} , and since the number of chaining mesh cells, N_{chain} scales with the problem size, the procedure reduces the operation count back to $O(N_{\text{grid}})$ scaling.

1.2.6 Enzo I/O

All input/output operations in **Enzo** are performed using the Hierarchical Data Format 5 library (HDF5). HDF5, specifically hdf5 v.1.6.5 has a number of very attractive features for management of large, complex data sets and the associated metadata. HDF5 has an excellent logical design and is available on every major computing platform in the NSF/DOE arena. One outstanding advantage of HDF5 is that one can easily re-start a model on a different computational platform without having to worry about differences in endianness or internal floating point format.

The basic data model in **Enzo** is that a given MPI task “owns” all of the I/O required by the set of top level grids and subgrids present in that task. A single method is used to provide checkpointing and re-start capability and for science dumps at specified intervals.

All I/O is designed for moving the largest possible amount of data per operation (subject to chunking constraints described below), and all memory references are stride 1 for maximum efficiency. Each task performs all of its I/O independently of the other tasks and there is no logical need for concurrency, i.e, there is actually no advantage to using the parallel co-operative interface available in HDF5. Although synchronization is not required in principle, it is convenient to synchronize all processes after an entire dump has been written so that it is safe to hand off to asynchronous processes which may move the data across a network or to archival storage.

The basic object in HDF5 is a file containing other HDF5 objects such as data sets and associated metadata attributes. HDF5 also supports a truly hierarchical organization through the group concept. **Enzo** uses each of these features. The group concept, in particular, allows **Enzo** to pack potentially huge numbers of logically separate groups of data sets (i.e. one such set for each subgrid) into a single Unix file resulting in a correspondingly large reduction in the number of individual files and making the management of the output at the operating system level more convenient and far more efficient. In an **Enzo** AMR application running on N processors with G subgrids per MPI task with each subgrid having D individual baryon field and/or particle lists this results in only N HDF5 files per data dump instead of $N \cdot G$ files without grouping or $N \cdot G \cdot D$ files in a simplistic case with no groups or data sets and a separate file for each physical variable.

The packed-AMR scheme necessarily involves many seek operations and small data transfers when the hierarchy is deep. A vital optimization in **Enzo** is the use of in-core buffering of the assembly of the packed-AMR HDF5 files. This is very simply achieved using the HDF5 routine `H5Pset_fapl_core` to set the in-core buffering properties for the file. **Enzo** uses a default buffer size

of 1 MByte per file. At present, in HDF5 v.1.6.5 this is only available on output where increases in performance by $> 120\times$ have been observed with *Lustre* file systems. The lack of input buffering implies that reading re-start files can be relatively expensive compared to writing such files but in a typical batch run there may be dozens of write operations for a single read operation in the re-start process. When input buffering becomes available in a future version of HDF5 the cost of I/O operations will be a negligible fraction of the run time even for extremely deep hierarchies.

For very large uniform grid runs (e.g., 2048^3 cells and particles) we encounter different problems. Here individual data sets are so large it is necessary to using chunking so that any individual read/write operation does not exceed certain internal limits in some operating systems. The simplest strategy is to ensure that access to such data sets is by means of HDF5 hyperslabs corresponding to a plane or several planes of the 3D data. For problem sizes beyond 1280^3 it is necessary to use 64-bit integers to count dark matter particles or compute top grid data volumes. *Enzo* uses 64-bit integers throughout so it is necessary to handle MPI and HDF5 integer arguments by explicitly casting integers back to 32-bits.

1.3 Performance and scaling on terascale platforms

Enzo has two primary usage modes: *unigrid*, in which a non-adaptive uniform Cartesian grid is used, and *AMR*, in which adaptive mesh refinement is enabled in part or all of the computational volume. In actuality, unigrid mode is obtained by setting the maximum level of refinement to zero in an AMR simulation, and precomputing the relationships between the root grid tiles. Otherwise, both calculations using the same machinery in *Enzo* and are updated according to Fig. 1.2. The scaling and performance of *Enzo* is very different in these two modes, as are the memory and communication behaviors. Therefore we present both in this section.

1.3.1 Unigrid application

Fig. 1.4(a) shows the results of a recent unigrid simulation carried out on 512 processors of NERSC *bassi*, and IBM Power5 system. The simulation was performed on a grid of 1024^3 cells and the same number of dark matter particles. The simulation tracked 6 ionization states of hydrogen and helium including nonequilibrium photoionization and radiative cooling. Fig. 1.4(a) plots the total wall-clock time per timestep versus timestep as well as the cost of major code regions corresponding to the procedure calls in Fig. 1.2. Unigrid performance is quite predictable, with the cost per timestep for the

different code regions being roughly constant. In this example hydrodynamics dominates the cost of a timestep (45%). The remaining cost breaks down as follows: radiative cooling (15%), boundary update 2 (11%), self-gravity (7%), boundary update 1 (7%), rate equations (3%). An additional 12% is spent in message passing. Fig. 1.4(b) shows the CPU time per processor for the job. We find that the master processor in each 8 processor SMP node is doing 9% more work than the other seven, otherwise the workload is nearly uniform across processors.

1.3.2 AMR application

Fig. 1.5(a) plots the wall-clock time per root grid timestep versus timestep for an AMR simulation with identical cosmology and physics as our unigrid example, only here the base grid has dimensions 512^3 and up to 4 levels of refinement are permitted in dense regions. Prior to the onset of mesh refinement at timestep 103 the AMR simulation behaves identically to a unigrid simulation, with hydrodynamics dominating the cost per timestep. By timestep 156, the cost of a root grid timestep has increased one hundred-fold. There are several reasons for this. First, we use hierarchical timestepping in **Enzo**, which means that for each root grid timestep, a subgrid of level ℓ will be timestepped roughly 2^ℓ times. The total number of substeps per root grid timestep for a fully refined region is $\sum_{\ell=1}^{\ell_{max}} 2^\ell$, which is 30 for $\ell_{max}=4$. By timestep 156, only a small fraction of the total volume is refined, and the average number of substeps per root grid timestep is 8, far less than the factor 100 we observe. The dominant cause for the upturn is the cost of procedure **boundary_update_2**, which exchanges ghost zone data between every subgrid at every level and substep. Secondary causes for the upturn are the procedures **rate_equations** and **radiative_cooling**. These routines are both subcycled on a chemical timescale that is short compared to the hydrodynamic time step. The separation between these two timescales increases as the gas density increases. AMR allows the gas to become very dense, and thus the ionization of cooling calculations grows to dominate the hydrodynamics calculation.

Fig. 1.5(b) shows the cumulative CPU time as a function of processor number. There is considerably more spread between the largest and smallest time (30000/10000=3) compared with the unigrid run (5800/4800=1.21). This is due to true load imbalances arising from mesh refinement, chemistry/cooling subcycling, and communication loads. At present our dynamic load balancing algorithm in **Enzo** only tries to equalize the zone-timesteps among processors. It does not attempt to balance communications and subcycling loads. This is an obvious area for improvement.

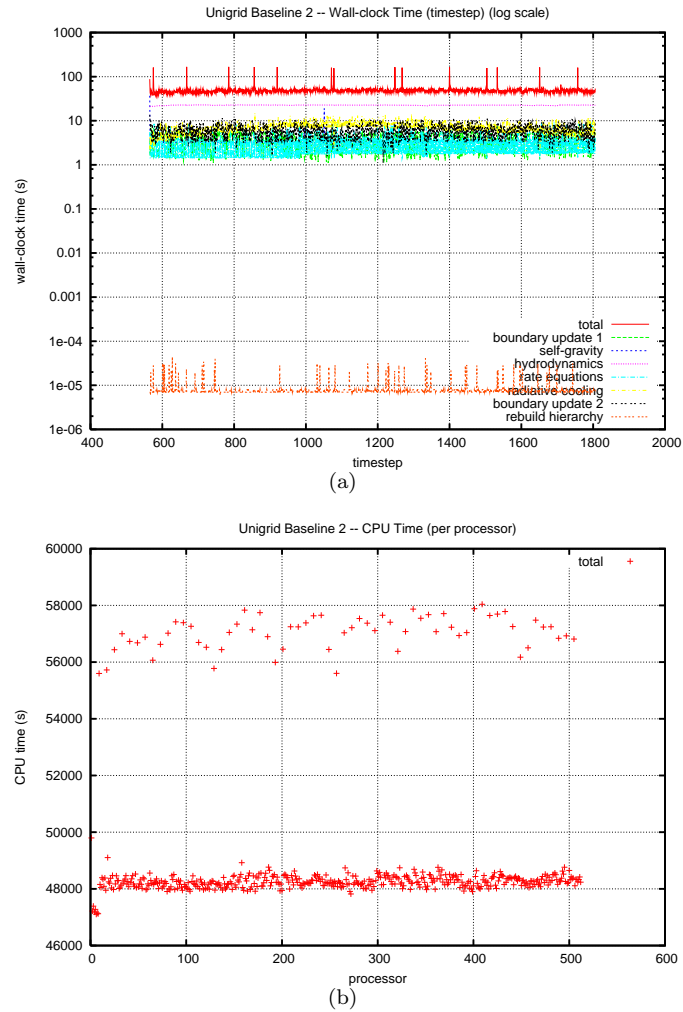


FIGURE 1.4: (a) Wall-clock time per timestep versus timestep broken down according to major code region for the 1024^3 unigrid simulation. Spikes in total time correspond to I/O events.; (b) CPU time per processor versus processor. Simulations were carried out on 512 cpus on NERSC IBM Power 5 system *Bassi*.

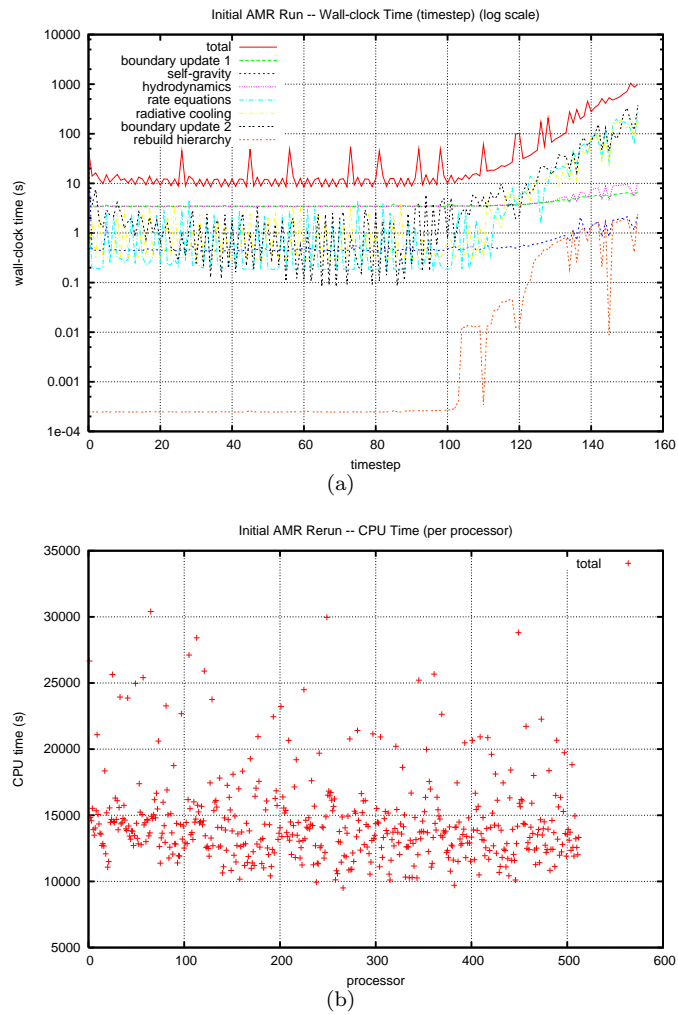


FIGURE 1.5: (a) Wall-clock time per root grid timestep versus root grid timestep broken down according to major code region for the 512^3 4-level AMR simulation; (b) CPU time per processor versus processor. Simulations were carried out on 512 cpus on NERSC IBM Power 5 system *Bassi*.

1.3.3 Parallel scaling

Because the cost per timestep of a unigrid simulation is roughly constant, varying by only a factor of a few as physical conditions change, parallel scaling tests are easy to perform for even the largest grids and particle counts. The same is not true of AMR simulations since the load is constantly changing in a problem-dependent way. Time-to-solution is the only robust metric. Because large AMR simulations are so costly, it is not possible to run many cases to find the optimal machine configuration for the job. Consequently we do not have parallel scaling results for AMR simulations of the size which require terascale platforms (for smaller scaling tests, see [11].) In practice, processor counts are driven by memory considerations, not performance. We expect this situation to change in the petascale era where memory and processors will be in abundance. Here, we present our unigrid parallel scaling results for *Enzo* running on a variety of NSF terascale systems available to us.

Figure 1.6 shows the results of strong scaling tests of *Enzo* unigrid simulations of the type described above for grids of size 256^3 , 512^3 , 1024^3 and 2048^3 and an equal number of dark matter particles. We plot cell updates/sec/cpu versus processor count for the following machines: *Lemieux*, a Compaq DEC alpha cluster at PSC, *Mercury*, an IBM Itanium2 cluster at NCSA, and *DataStar*, an IBM Power4 cluster at SDSC. Ideal parallel scaling would be horizontal lines for a given architecture, differentiated only by their single processor speeds. We see near-ideal scaling for the 256^3 test on *DataStar* and *Lemieux* up to 32 processors, followed by a gradual roll-over in parallel performance to $\sim 50\%$ at 256 processors. Nonideality sets in at 16 processors on *Mercury*, presumably due to its slower communications fabric. As we increase the problem size on any architecture, parallel efficiency increases at fixed NP, and the roll-over moves to higher NP. Empirically, we find that parallel efficiency suffers if grid blocks assigned to individual processors are smaller than about 64^3 cells. Using blocks of size $128^2 \times 256$, we find that the cell update rate for our 2048^3 simulation on 2048 *DataStar* processors is $\sim 80\%$ the cell update rate of our 256^3 on 4 processors. *Enzo* in unigrid mode is very scalable.

1.4 Toward petascale *Enzo*

1.4.1 New AMR data structures

For moderate numbers of processors, the current datastructure used for storing the AMR grid hierarchy is adequate. Even though the hierarchy topology is stored redundantly on each processor, because the data fields are vastly larger than *Enzo*'s individual C++ `grid` objects, the extra memory overhead involved is insignificant. However, as the number of processors increases, this

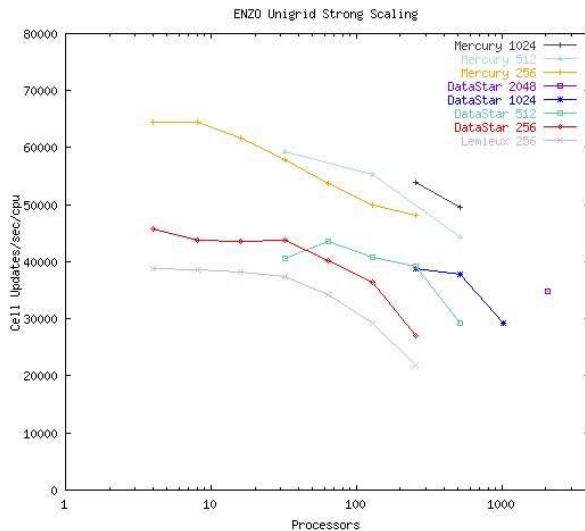


FIGURE 1.6: Enzo strong scaling results for unigrid cosmology runs of size 256^3 , 512^3 , 1024^3 and 2048^3 on NSF terascale platforms.

memory overhead increases as well. For the processor counts required for petascale-level computing, the storage overhead would overwhelmingly dominate, to the point where the largest computation would actually not be limited by the number of processors, but rather by the amount of memory available for each processor. Thus, for **Enzo** to scale to the petascale level, the memory overhead for storing the AMR hierarchy must be reduced.

The memory required for storing **Enzo**'s current AMR datastructure can be approximated as $|F| + np|G|$, where the first term $|F|$ is the field variable data, and the second term $np|G|$ is the overhead for storing the grid hierarchy datastructure. Here n is the number of grid patches, p is the number of processors, and $|G|$ is the storage required by a C++ `grid` object.

One approach to reducing the size of the overhead term $np|G|$ is to reduce the size of the `grid` object by removing unnecessary member variables from the `grid` class. Since some member variables are constant for a hierarchy level, and some are constant for the entire hierarchy, the amount of memory required would be reduced. This refactoring is indicated by the first transition in Figure 1.7. Although this would indeed save some memory, preliminary estimates indicate that the savings would only be about 13.5%.

A second approach to reducing the size of the overhead term would be to split the `grid` class into two subclasses `grid_local` and `grid_remote`, and use `grid_local` objects for local grids that contain field data, and `grid_remote` objects for grid patches whose data fields reside on another processor. This refactoring is indicated by the second transition in Figure 1.7. This modifica-

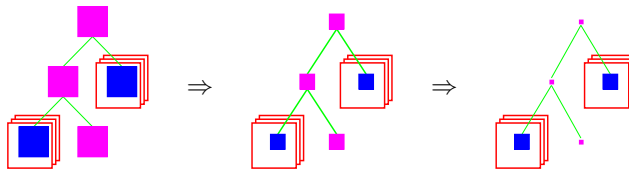


FIGURE 1.7: Reducing AMR datastructure storage overhead. Solid blue squares represent local `grid` objects, solid magenta squares represent remote `grid` objects, and open red boxes represent data fields. The first transition illustrates reducing the size of all `grid` objects, and the second transitions illustrates splitting the single `grid` class into two `grid_local` and `grid_remote` subclasses.

tion would change the overhead storage term from $np|G|$ to $n((p-1)|G_r| + |G_l|)$, where $|G_r|$ is the size of the `grid_remote` class and $|G_l|$ is the size of the `grid_local` class. The advantage of doing this is that the `grid_remote` class could be made much smaller, since most of the variables in the `grid` class are only required for local grids. Also, a vast majority of the grid classes are these much smaller `grid_remote` objects. Thus the memory savings for this modification would be quite large—a factor of roughly 14 over the already slightly reduced `grid` size from the first approach.

1.4.2 Hybrid parallelism

Another improvement would of course be not to store the entire grid hierarchy on each processor. The easiest approach would be to store one copy per shared memory node, which would decrease the memory storage further by a factor equal to the number of processors per node. This could be implemented with a hybrid parallel programming model in which instead of assigning one MPI task per processor which serially executes its root grid tile and all its subgrids, we assign one MPI task per node. This heavy weight node would execute a somewhat larger root grid tile and its more numerous subgrids, using shared memory parallelism wherever possible. For example, every subgrid at a given level of refinement would be processed concurrently using OpenMP threads [12].

While the above modifications to the AMR datastructure should allow `Enzo` to run on machines with on the order of 10^4 to 10^5 processors, extending to 10^6 processors would require reducing the overhead even further. The ultimate improvement memory-wise would be to store a single copy of the grid hierarchy, though depending on the node interconnect that would cause a communication bottleneck. A refinement on this approach would be to store one copy of the hierarchy for every M processors, where M is some machine-dependent number chosen to balance the tradeoff between memory

and communication overhead.

1.4.3 Implicitly-coupled radiation hydrodynamics

We are working to incorporate radiation transfer processes within the **Enzo** framework to improve the physical realism of cosmological modeling of self-regulated star formation and predictions on the epoch of cosmic re-ionization. These efforts are unique within the computational astrophysics community, because unlike traditional approaches to such multi-physics couplings, we are coupling the radiation transfer implicitly with both the fluid energy and chemical kinetics processes. This approach promises to provide a fully-consistent coupling between the physical processes, while enabling the use of highly scalable solvers for the coupled solution.

Through implicitly coupling the radiation-hydrodynamics-chemical kinetics processes together, we have the benefits of numerical stability in time (regardless of step size) and the ability to use high-order time discretization methods. On the other hand, this coupling results in a nonlinear system of partial differential equations that must be solved at each time step. For this coupled solution we will use *Inexact Newton Methods*, which in recent years have been shown to provide an efficient and scalable approach to solving very large systems of nonlinear equations [13, 14]. This scalability arises due to a number of factors, notably the fact that for many problems Newton’s method exhibits a convergence rate that is independent of spatial resolution, so long as the inner linear solver scales appropriately [15]. As radiation diffusion processes are elliptic in nature, and radiative couplings to fluid energy and chemical kinetics occur only locally, we plan to achieve such optimal scalability in the linear solver through the use of a Schur Complement formulation ([16]) to reduce the coupled Newton systems to scalar diffusion problems, which will then be solved through optimally scalable multi-level methods, provided by the state-of-the-art HYPRE linear solver package [17, 18]. This solver library has been shown to scale up to massively parallel architectures ([19]), and as the computational heart of the Inexact Newton approach is the inner linear solver, we are confident that such an implicit formulation and solution will enable radiation-hydrodynamics-chemical kinetics simulations in **Enzo** to the Petascale and beyond.

1.4.4 Inline analysis tools

Petascale cosmology simulations will provide significant data analysis challenges, primarily due to the size of simulation datasets. For example, an **Enzo** Lyman alpha forest calculation on a 1024^3 grid, the current state-of-the-art, requires approximately 110 GB of disk space per simulation output. Tens or hundreds of these outputs are required per simulation. If scaled to a 8192^3 grid, a reasonable size for a petascale computation, this would result in 56 TB of data per simulation output, and multiple petabytes of data written to

disk in total. Given these dataset sizes, analysis can become extremely time-consuming: doing even the simplest post facto analysis may require reading petabytes of data off of disk. For more complex analysis, such as spectrum or N-point correlation function generation, the data analysis may be comparable in computational cost to the simulation itself. Analysis tools for petascale datasets will by necessity be massively parallel, and new forms of data analysis that will be performed hundreds or thousands of times during the course of a calculation may make it exceedingly cumbersome to store all of the data required. Furthermore, it will become extremely useful to be able to monitor the status and progress of petascale calculations as they are in progress, in an analogous way to more conventional experiments.

For these reasons, among others, doing data analysis while the simulation itself is running will become necessary for petascale-level calculations. This will allow the user to save disk space and time doing I/O, greatly enhance the speed with which simulations are analyzed (and hence improve simulation throughput), and have access to data analysis strategies which are otherwise impractical or impossible. Analysis that can be done during cosmological simulations include the calculation of structure functions and other global snapshots of gas properties; dark matter power spectra, halo and substructure finding, and the generation of merger trees; radial profile generation of baryon properties in cosmological halos; production of projections, slices, and volume-rendered data for the creation of movies; the generation of synthetic observations, or “light cones”; the calculation of galaxy population information such as spectral energy distributions and color-magnitude relations; global and halo-specific star formation rates and population statistics; ray tracing for strong and weak lensing calculations and for Lyman alpha forest or DLA spectrum generation; and essentially any other type of analysis that can be massively parallelized. Analysis of simulations in this way, particularly if done with greater frequency in simulation time, may enhance serendipitous discovery of new transient phenomena.

A major constraint to inline analysis of cosmological simulations is that it requires very careful and possibly time-consuming planning on the part of the scientists designing the calculation, and is limited to analysis techniques that can be heavily parallelized. As a result, inline analysis techniques will not completely negate the necessity of writing out significant amounts of data for follow-up analysis and data exploration. Furthermore, inline analysis will require careful integration of analysis tools with the simulation code itself. For example, the simulation and analysis machinery will, for the sake of efficiency, require shared code, data structures, and parallelization strategies (i.e. domain-decomposed analysis if the simulations are similarly decomposed). If these relatively minor hurdles can be surmounted, however, this sort of analysis will result in gains far beyond the additional computational power used.

1.5 Acknowledgements

Enzo has been developed with the support of the National Science Foundation via grants ASC-9318185, AST-9803137, AST-0307690, and AST-0507717; the National Center for Supercomputing Applications via PACI Subaward ACI-9619019; and the San Diego Supercomputer Center via the Strategic Applications Partners program. Greg Bryan acknowledges support from NSF grants AST-05-07161, AST-05-47823 and AST-06-06959.



References

- [1] Spergel, D. N. *et al.*, Wilkinson Microwave Anisotropy Probe (WMAP) Three Year Results: Implications for Cosmology, eprint arXiv astro-ph0603449, 2006.
- [2] Enzo home page <http://lca.ucsd.edu/portal/software/enzo>
- [3] P. Anninos, Y. Zhang, T. Abel, and M. L. Norman. Cosmological hydrodynamics with multi-species chemistry and nonequilibrium ionization and cooling. *New Astronomy*, 2:209–224, August 1997.
- [4] G. L. Bryan, M. L. Norman, J. M. Stone, R. Cen, and J. P. Ostriker. A piecewise parabolic method for cosmological hydrodynamics. *Comp. Phys. Comm.*, 89:149–168, 1995.
- [5] R. W. Hockney and J. E. Eastwood. *Computer Simulation Using Particles*. IOP Publishing, Bristol and Philadelphia, 1988.
- [6] M. J. Berger and P. Colella. Local adaptive mesh refinement for shock hydrodynamics. *J. Comp. Phys.*, 82:64–84, 1989.
- [7] G. L. Bryan. Fluids in the universe: Adaptive mesh in cosmology. *Computing in Science and Engineering*, 1:2:46, 1999.
- [8] MPI homepage <http://www-unix.mcs.anl.gov/mpi/>
- [9] HDF homepage <http://www.hdfgroup.org>
- [10] Z. Lan, V. Taylor, and G. Bryan. Dynamic Load Balancing for Structured Adaptive Mesh Refinement Applications Proc. of 30th Int. Conference on Parallel Processing 2001, Valencia, Spain
- [11] J. Bordner, A. Kritsuk, M. Norman and R. Weaver. Comparing Parallel CAMR and SAMR Hydrodynamic Applications. *SIAM J. Sci. Comp.*, submitted, 2007.
- [12] OpenMP homepage <http://www.openmp.org>
- [13] D. A. Knoll, and D. E. Keyes. Jacobian-free Newton–Krylov methods: a survey of approaches and applications. *J. Comp. Phys.*, 193:357–397, 2004.
- [14] D. E. Keyes, D. R. Reynolds and C. S. Woodward. Implicit solvers for large-scale nonlinear problems. *J. Phys.: Conf. Ser.*, 46:433–442, 2006.

- [15] M. Weiser, A. Schiela and P. Deuffhard. Asymptotic mesh independence of Newton's method revisited. *SIAM J. Numer. Anal.*, 42:1830–1845, 2005.
- [16] P. N. Brown and C. S. Woodward. Preconditioning strategies for fully implicit radiation diffusion with material-energy coupling. *SIAM J. Sci. Comput.*, 23:499–516, 2001.
- [17] R. D. Falgout and U.M. Yang. hypre: a Library of High Performance Preconditioners, in Computational Science – ICCS 2002 Part III. Springer-Verlag, 632–641, 2002.
- [18] HYPRE homepage http://www.llnl.gov/casc/linear_solvers
- [19] A. H. Baker, R. D. Falgout and U. M. Yang. An Assumed Partition Algorithm for Determining Processor Inter-Communication. *Parallel Computing*, 32:319–414, 2006.

